



Cite this: Dalton Trans., 2025, 54, 6876

The crucial role of acetonitrile in the mechanism of Pd(II)-catalyzed activation of polar vinyl monomers[†]

Chiara Alberoni, ^{‡,a} Esaïe Reusser, ^b Gabriele Balducci, ^a Enzo Alessio, ^a Martin Albrecht ^{*,b} and Barbara Milani ^{*,a}

The migratory insertion reaction of a polar vinyl monomer into the Pd–alkyl bond and the chain walking process are two of the key steps in the catalytic cycle for the synthesis of functionalized polyolefins through coordination/insertion polymerization. Here, we present a detailed NMR investigation to gain insight into these fundamental steps and demonstrate the critical role of traces of MeCN in this process. We used Pd(II) complexes containing a N–N' bidentate pyridyl-pyridylidene amide (py-PYA) ligand, which are known to cooligomerize ethylene and methyl acrylate (MA). The reaction of three related Pd–(py-PYA) complexes, *viz.* neutral $[\text{Pd}(\text{CH}_3)\text{Cl}(\text{py-PYA})]$, **1a**, and cationic derivatives $[\text{Pd}(\text{CH}_3)(\text{NCCCH}_3)(\text{py-PYA})]\text{X}$, $\text{X} = \text{BF}_3$ **1b** and PF_6 **1c**, with either MA or *N,N*-dimethylacrylamide (DMA), showed distinct reactivity with the two polar monomers. While 4-, 5-, and 6-membered palladacycles, resulting from the migratory insertion reaction of the polar monomer into the Pd–CH₃ bond and subsequent chain walking, were detected with both monomers, their amounts varied considerably with the type of polar monomer, the anion, and the amount of MeCN. Specifically, we found that the coordinating ability of MeCN plays a critical and ambivalent role: on one hand, it hampers the coordination and insertion of the polar olefin, and on the other hand, it markedly suppresses the chain walking process. Moreover, we report here the first solid state structure of a 5-membered metallacyclic species derived from DMA insertion into the Pd–CH₃ bond. The palladacyclic complexes are remarkably robust towards ethylene, though they react with carbon monoxide to form the palladium acyl species, opening perspectives for these complexes to catalyze CO/DMA copolymerization.

Received 12th February 2025,
Accepted 17th March 2025

DOI: 10.1039/d5dt00340g
rsc.li/dalton

1. Introduction

The efficient synthesis of functionalized polyolefins through the direct, controlled, and homogeneously catalyzed copolymerization of ethylene with polar vinyl monomers remains an unsolved problem in the field of polymer chemistry.^{1–5} For potential industrial exploitation, in addition to finding a catalyst with sufficiently high activity, the chain walking process needs to be controlled to tune the microstructure of the produced macromolecules.^{6,7} Indeed, this process is in

competition with the insertion of a new monomer molecule into the growing polymer chain and it can occur after the insertion of both ethylene and the polar monomer. In the first case, it determines the branching density of the obtained macromolecule, whereas in the second case, it is responsible for locating the polar monomer at the end of the branches (Scheme 1). These two features contribute significantly to the definition of the chemical, physical, and mechanical properties of the produced polymer and consequently its potential applications.

Two types of Pd(II) catalysts have mainly been investigated for the copolymerization of ethylene with industrially relevant polar vinyl monomers, such as acrylic esters and acrylamides. One is based on α -diimine chelates (N–N, **L1**, Chart 1) that typically lead to branched macromolecules with a low content of the polar monomer, inserted preferentially at the end of the branches as a result of the chain walking process.^{8–10} The other contains phosphino-sulfonate chelates (P–O, **L2**, Chart 1) that promote the formation of linear copolymers with a high content of the polar monomer inserted into the main chain (almost in a 1 : 1 ratio with ethylene).^{11,12}

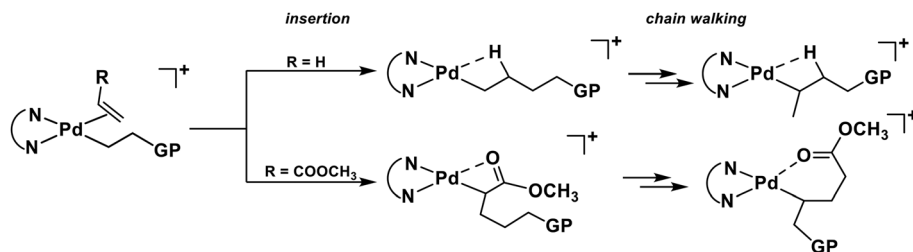
^aDipartimento di Scienze Chimiche e Farmaceutiche, Università di Trieste, Via Licio Giorgieri 1, 34127 Trieste, Italy. E-mail: milaniba@units.it

^bDepartment of Chemistry, Biochemistry and Pharmaceutical Sciences, University of Bern, Freiestrasse 3, CH-3012 Bern, Switzerland. E-mail: martin.albrecht@unibe.ch

[†]Electronic supplementary information (ESI) available: NMR spectra of the investigated reactions and detected intermediates and crystallographic data for the complex *trans*-MC5^{DMA}. CCDC 2386206. For ESI and crystallographic data in CIF or other electronic format see DOI: <https://doi.org/10.1039/d5dt00340g>

[‡]Current address: Dipartimento di Scienze Chimiche, Università degli Studi di Padova, Via F. Marzolo 1, 35121 Padova, Italy.





Scheme 1 The chain walking process taking place after the insertion of ethylene (top) and methyl acrylate (bottom). GP = growing polymer chain.

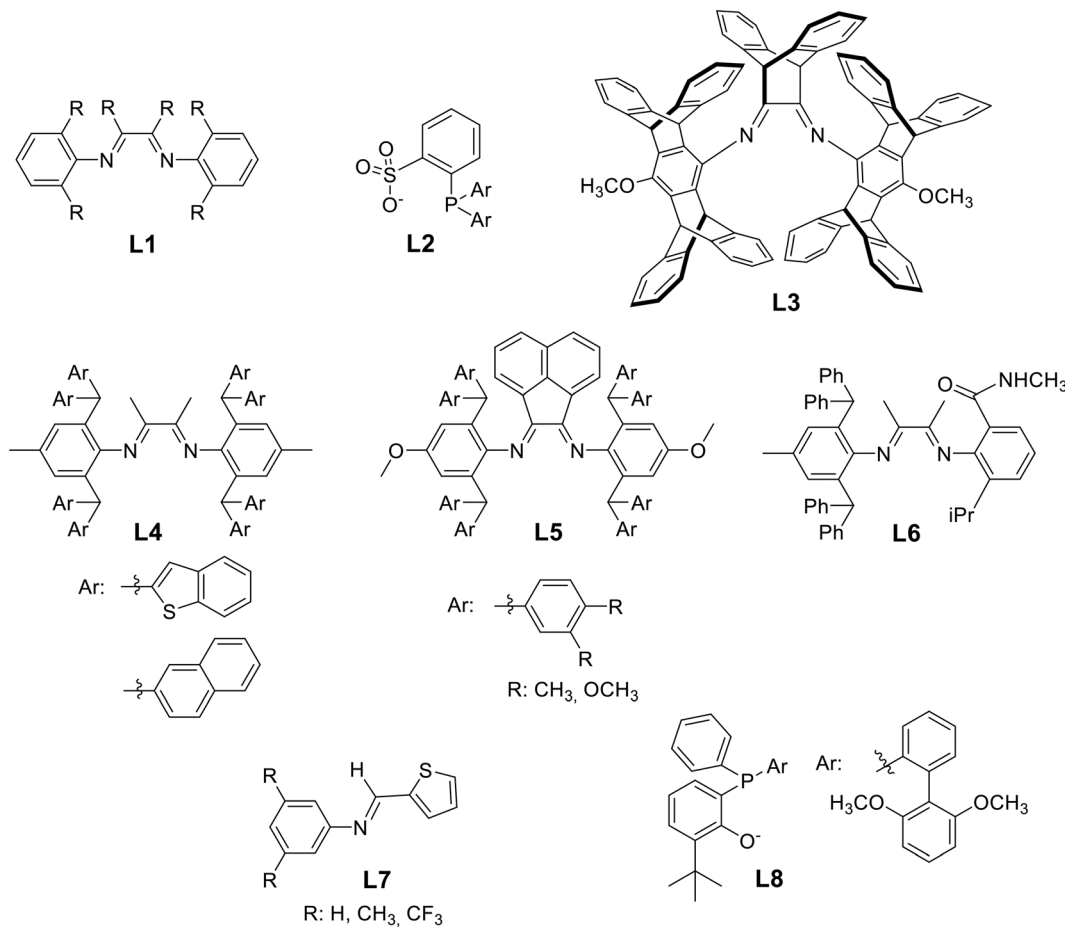


Chart 1 Examples of families of ancillary ligands reported in the literature for Pd-catalyzed copolymerization of ethylene and polar vinyl monomers.

Following Brookhart's seminal work,⁸ the control of copolymer topology was mainly addressed through modifications of the N–N structure.^{13,14} For instance, the highly encumbered α -diimine **L3** (Chart 1) produced hyperbranched copolymers with the polar monomer inserted into the main chain.^{15,16} This way of enchainment of methyl acrylate (MA), which is atypical for a Pd-catalyst based on α -diimines, originates from a change in the insertion regiochemistry from the usual 2,1 to 1,2 fashion, hampering the chain walking process after polar monomer insertion.

With the purpose of slowing down the chain walking process, highly hindered substituents were introduced at the *ortho* posi-

tions of the aryl rings, and the diaryl methyl fragment emerged as the preferred common motif (**L4** derivatives in Chart 1).^{17,18} This motif has also been very recently applied to Pd-catalysts containing α -diimines with the acenaphthene skeleton, **L5**.¹⁴

Another approach involves the introduction of specifically functionalized groups on the N–N chelate, such as a benzothiophene in **L4** or an imide functionality in **L6** (Chart 1).^{19–21} The former, through an interaction of the sulfur atom of **L4** with the β -CH moiety of the growing copolymeric chain, inhibited β -H elimination, thereby suppressing both the chain walking process and the chain transfer reaction. Conversely, the

H-bond donor properties of **L6** assisted the insertion of MA into the Pd-alkyl bond and promoted the opening of the metalacycle intermediate obtained after MA insertion.

In line with these findings, we reported that also the introduction at one of the coordination sites of the Pd center of a hemilabile, potentially bidentate ligand, such as a thiophenimine **L7**, affected the way of the polar monomer enchainment (Chart 1).²² Methyl acrylate was inserted both in the main chain and at the end of the branches of the copolymers depending on both the solvent used for the catalysis and the substituents on ligand **L7**. An in-depth NMR study highlighted that **L7** remained in close proximity to the metal ion, favoring the formation of an open-chain intermediate, which slowed down the chain walking process and trapped the polar monomer into the copolymer main chain.

Acrylamides, *e.g.* *N,N*-dimethylacrylamide (DMA), constitute another family of polar vinyl monomers of industrial interest.^{23,24} Ethylene/acrylamide copolymers were produced with Pd(II) catalysts bearing P-O chelates (**L2**, Chart 1), but not with α -diimine ligands. The polar monomer was incorporated both in the main chain and in unsaturated chain ends, suggesting that β -H elimination takes place after DMA insertion.²³ Similarly, a neutral Ni(II) complex with the P-O chelate **L8** was effective in ethylene/DMA copolymerization, achieving 3.3 mol% DMA incorporation.²⁵ The high steric hindrance around the Ni center was suggested to disfavor the β -H elimination reaction and the formation of deactivated dinuclear species, leading to increased activity and high molecular weight of the obtained copolymers.

In an effort to combine the different donor motifs of P-O chelates and the benefits of N-N α -diimines, we developed disymmetric N-N'-pyridyl-substituted pyridylidene amide (py-PYA) chelates such as **L9** for ethylene/MA copolymerization (Chart 2).²⁶ In particular, the coordination/insertion reaction of both ethylene and the polar monomer was favored with the *ortho*-pyridylidene system *o*-**L9**, in which the pyridinium heterocycle is twisted out of the metal coordination plane. This structural feature resulted in a pronounced anionic character of the PYA nitrogen donor atom and thus increased the electron density on the palladium

ion,²⁷ a feature that according to the literature enhances catalytic performances compared to Brookhart's catalyst for ethylene/methyl acrylate copolymerization.^{28,29}

However, the productivity of Pd(II) catalysts with py-PYA ligands was low and the increase of the steric hindrance around the metal center was considered an advantageous approach for obtaining better performing catalysts. Thus, the new py-PYA ligand **L10** was synthesized, introducing an additional methyl group on the 3-position of the PYA ring (Chart 2).³⁰ The corresponding palladium(II) complex, $[\text{Pd}(\text{CH}_3)(\text{NCCH}_3)(\text{L10})]^+$, reached a productivity of 26.6 g of polymer per g of Pd, affording unsaturated esters together with significant amounts of ethylene/MA cooligomers. *In situ* NMR investigations showed for the first time the presence of a 4-membered palladacycle (**MC4^{MA}**), originating from migratory insertion of MA into the Pd-CH₃ bond. Over time, part of the **MC4^{MA}** intermediate evolved into the corresponding 5-membered palladacycle **MC5^{MA}**, but did not proceed further to the commonly observed 6-membered palladacycle, thus indicating that the chain walking process is very slow and it is in competition with β -H elimination, leading to the formation of methyl crotonate, **MeCr** (Scheme 2).³⁰

Due to the importance of the chain walking process in determining the polymer microstructure,^{6,7,14,31} we aimed to gain further insight into the parameters that control this reactivity. A particular focus is directed towards the possibility to tune the availability of a coordination site on palladium, which is required for chain walking (Scheme 1). Specifically, we investigated the critical role of several factors including the nature of the counterion, the coordinating ability of the polar monomer, and – in particular – the relevance of stoichiometric amounts of MeCN. With this aim, we performed detailed *in situ* NMR studies on the reaction of both cationic $[\text{Pd}(\text{CH}_3)(\text{NCCH}_3)(\text{L10})]^+$ and *in situ* activated neutral $[\text{Pd}(\text{CH}_3)\text{Cl}(\text{L10})]$ complexes with polar vinyl monomers MA and DMA, by varying the above mentioned parameters. These insights provide guidelines for tailoring monomer insertion and for controlling linear *vs.* branched polymer structures.

2. Results and discussion

The reaction of ligand **L10** with $[\text{Pd}(\text{cod})(\text{CH}_3)\text{Cl}]$ afforded the neutral complex $[\text{Pd}(\text{CH}_3)\text{Cl}(\text{L10})]$ (**1a**) in excellent isolated

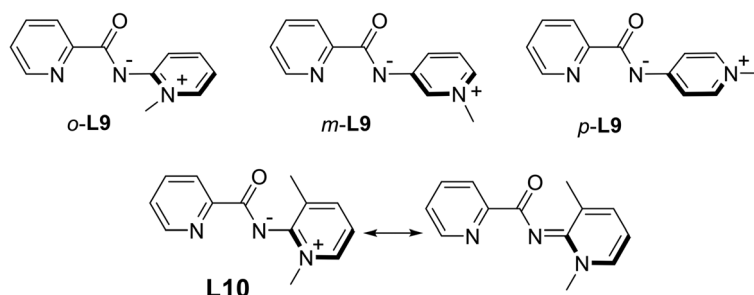
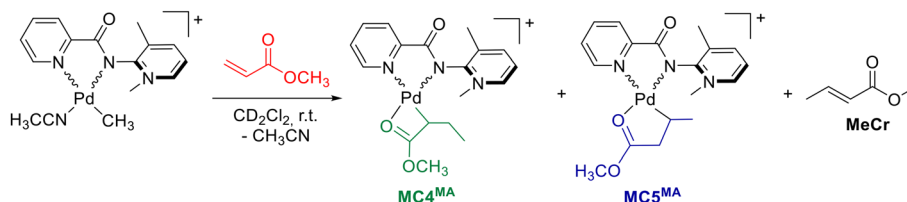


Chart 2 N–N'-pyridyl-pyridylidene amide (py-PYA) ligands **L9** and **L10**. The limiting resonance structures for **L10** are shown. The formal charges on ligand atoms are shown to highlight the zwitterionic form of the ligand; conventionally, no local charges are drawn.²⁷





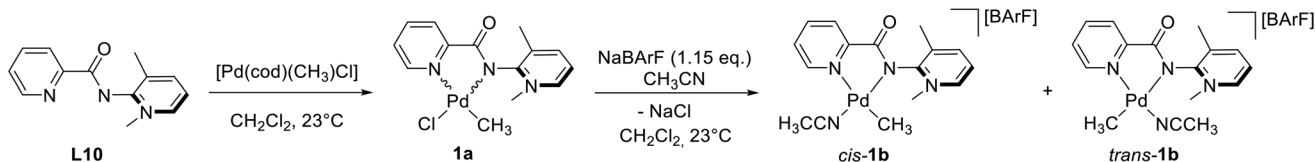
Scheme 2 Formation of 4-membered metallacycle **MC4^{MA}** upon methyl acrylate (MA) insertion into the Pd–Me bond in a Pd(py-PYA) complex and formation of **MC5^{MA}** upon chain walking and methyl crotonate (**MeCr**) from β -H elimination.

yields (92%, Scheme 3).³² In the presence of a small excess of sodium tetrakis[3,5-bis(trifluoromethyl)phenyl]borate NaBArF, **1a** was converted into the cationic solvento complex [Pd(CH₃)(NCCH₃)(L10)][BArF] (**1b**) in good yields (78%). Both complexes are air and moisture stable.

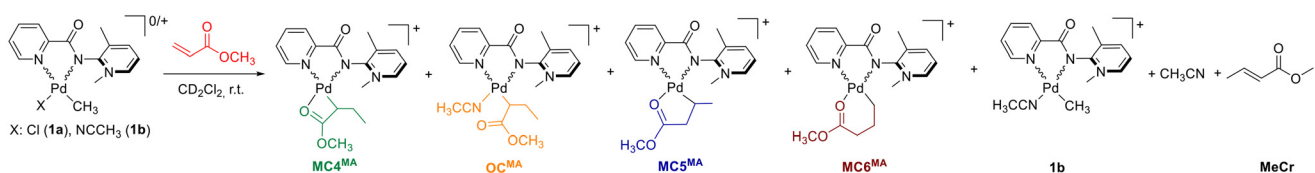
Characterization of the complexes by NMR spectroscopy revealed two sets of signals – attributed to the *cis* and *trans* isomers – both for **1a** and **1b**. The two isomers can be easily distinguished by their distinct Pd–CH₃ singlets, which appear *ca.* 1 ppm apart. The *cis* descriptor is attributed here to the isomer featuring the Pd–CH₃ group *cis* to the PYA nitrogen and *trans* to the pyridyl nitrogen (Scheme 3). In both complexes, NOE analysis indicated that the *cis* isomer is the major species, with a 4 : 1 *cis/trans* ratio in **1a** and a 19 : 1 ratio in **1b**. In the *cis* isomer of **1b**, due to the shielding effect of the adjacent PYA ring, the Pd–CH₃ group resonates at a much lower frequency, $\delta_{\text{H}} = -0.06$ ppm, than in the *trans* analogue, $\delta_{\text{H}} = +1.02$ ppm (CD₂Cl₂ solution, Fig. S1 and S2[†]). The large preference for the *cis* isomer in both **1a** and **1b** indicates that the PYA nitrogen exerts a considerably stronger *trans* influence than the pyridyl moiety. In addition, due to the out-of-plane orientation of the unsymmetrical PYA ring, the coordination plane is not a symmetry element, and thus these complexes are planar chiral, yet they form as racemates.

In the first series of experiments aimed at elucidating the reactivity of these complexes towards polar comonomers, 2 equiv. of MA and 1 equiv. of NaBArF were simultaneously

added to a CD₂Cl₂ solution of **1a** (Scheme 4). The ¹H NMR spectrum recorded immediately after the addition showed no residual signals for complex **1a** (both isomers), indicating its full conversion into three new species (Fig. S3[†]) identified as the 4-, 5- and 6-membered metallacycles (**MC4^{MA}**, **MC5^{MA}**, and **MC6^{MA}**, respectively), resulting from the migratory insertion reaction with the secondary regiochemistry of MA into the Pd–CH₃ bond of **1a** to yield **MC4^{MA}** followed by chain walking to afford **MC5^{MA}** and **MC6^{MA}** (Scheme 4 and Table 1). The resonances were assigned on the basis of integration, signal multiplicity and two-dimensional NMR experiments (Fig. S4 and S5[†]). The NMR data indicate that for each detected palladacycle, only the *cis* isomer, identified as the species with the Pd–C bond adjacent to the pyridylidene-amide ring, was evident. In addition, for **MC4^{MA}** and **MC5^{MA}**, due to the planar chirality and the fact that the palladium-bound carbon atom (α C) is a stereogenic center, the presence of four – equally abundant – diastereomers for each metallacycle is expected. It is quite likely, however, that their proton NMR resonances might not be distinguishable. Two of such diastereomers – presumably characterized by the opposite chirality of α C – are clearly evident for **MC5^{MA}** in the ¹H NMR spectrum of the reaction mixture recorded after 5 min by the splitting of the α CH, β CH₃, and CH₂ resonances (Fig. S3[†]). It is noteworthy that small amounts of **MC4^{MA}** were detected only within the first 5 min of the reaction, whereas **MC5^{MA}** and **MC6^{MA}** were always present. The **MC4^{MA}** : **MC5^{MA}** : **MC6^{MA}** ratio changed from



Scheme 3 Synthesis of **1a** and **1b** (*cis* and *trans* isomers indicated for the cationic complex only).



Scheme 4 Products detected by *in situ* NMR spectroscopy from the reaction of the Pd complexes **1a** and **1b** with MA.

Table 1 Relative amounts, in mol%, of the compounds present in solution at $t = 1$ min after the addition of MA to each starting mixture

Starting mixture	MC4^{MA}	OC^{MA}	MC5^{MA}	MC6^{MA}	1b	Free CH ₃ CN
1a + NaBArF	16	—	15	69	—	—
1b	8	26	6	15	45	Yes
1a + NaBArF + CH ₃ CN (1 equiv.)	9	29	4	14	44	Yes
1a + NaBArF + CH ₃ CN (2 equiv.)	5	20	—	—	75	Yes

16 : 15 : 69 after 1 min to 0 : 15 : 85 after 150 min (Table S1†). The resonances of methyl crotonate (**MCr**) started to appear after about 30 min and slowly increased with time, together with the appearance of a fine dark precipitate of Pd(0).

Different results were found when the same experiment was performed with a solution of the cationic complex **1b** (Scheme 4 and Table 1). In the spectrum recorded 1 min after the addition of MA, the main resonances were due to residual **1b** (45%), **MC4^{MA}**, **MC6^{MA}**, free CH₃CN and a new species, whereas the signals of **MC5^{MA}** were almost negligible (Fig. S6†). The new species, rapidly growing with time, features a Pd-bound acetonitrile (singlet at 2.45 ppm) and was identified as the open-chain intermediate (**OC^{MA}**), generated by MeCN coordination to **MC4^{MA}** (Scheme 4). After 150 min, the **MC4^{MA}** : **OC^{MA}** : **MC5^{MA}** : **MC6^{MA}** ratio was 17 : 54 : 8 : 21, indicating that in **1b** the coordination of MA, the migratory insertion reaction, and especially the chain walking process are slower than on the neutral complex **1a** activated *in situ* with NaBArF (Table S1†). This difference in the rate is most likely due to the presence of the bound acetonitrile in **1b**, which occupies one of the coordination sites available for catalysis on palladium (Fig. 1). MA insertion in the complex [Pd(CH₃) (NCCH₃)(L10)][PF₆] (**1c**), which differs from **1b** only by the counterion (PF₆[−] instead of BArF), is even slower: **MC5^{MA}** is not detectable in the first 15 min and **MC6^{MA}** not at all during the first 10 h.³⁰ This observation is in agreement with the well-known positive effect of BArF with respect to PF₆[−] on catalyst activity.³³ Furthermore, the data indicate that chain walking is also affected by the nature of the counterion and is particularly slow with PF₆[−], presumably because of tighter ion pairing of

Open Access Article. Published on 18 March 2025. Downloaded on 1/26/2026 2:42:50 PM.
This article is licensed under a Creative Commons Attribution-NonCommercial 3.0 Unported Licence.

(CC) BY-NC

cating that in **1b** the coordination of MA, the migratory insertion reaction, and especially the chain walking process are slower than on the neutral complex **1a** activated *in situ* with NaBArF (Table S1†). This difference in the rate is most likely due to the presence of the bound acetonitrile in **1b**, which occupies one of the coordination sites available for catalysis on palladium (Fig. 1). MA insertion in the complex [Pd(CH₃) (NCCH₃)(L10)][PF₆] (**1c**), which differs from **1b** only by the counterion (PF₆[−] instead of BArF), is even slower: **MC5^{MA}** is not detectable in the first 15 min and **MC6^{MA}** not at all during the first 10 h.³⁰ This observation is in agreement with the well-known positive effect of BArF with respect to PF₆[−] on catalyst activity.³³ Furthermore, the data indicate that chain walking is also affected by the nature of the counterion and is particularly slow with PF₆[−], presumably because of tighter ion pairing of

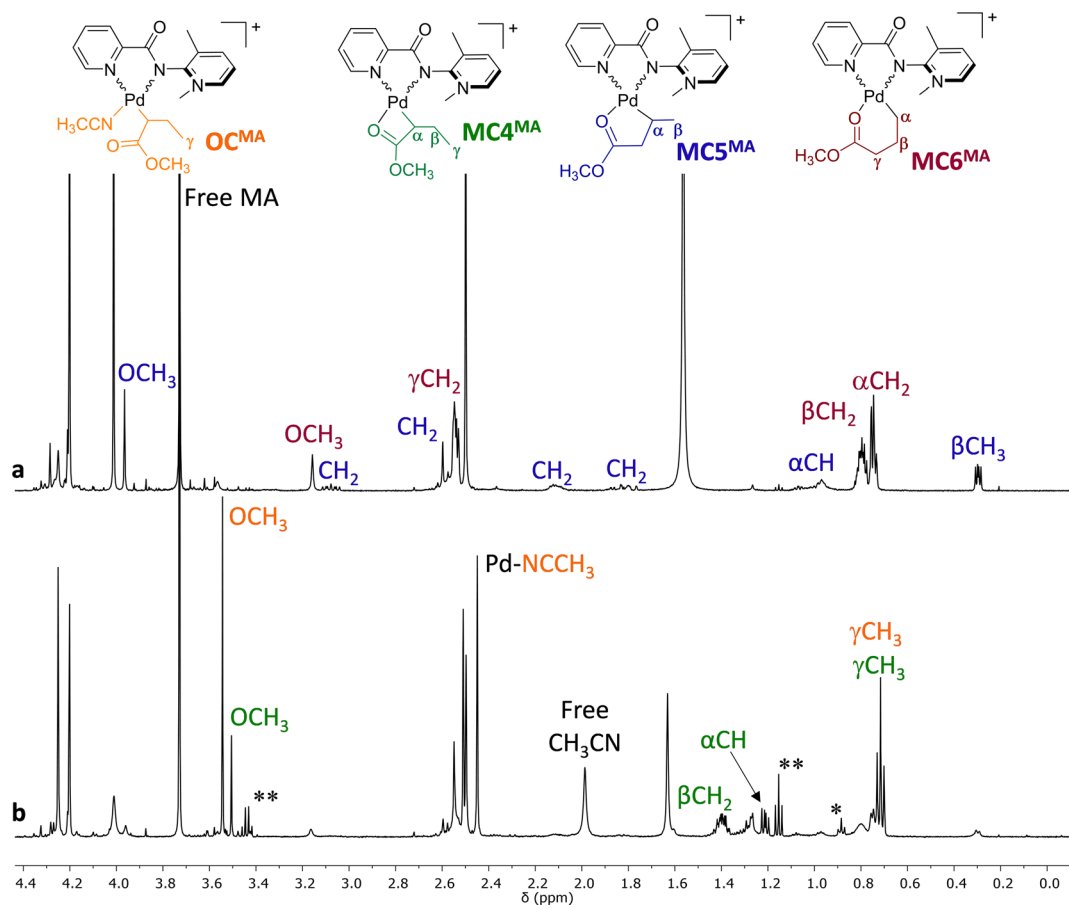


Fig. 1 ¹H NMR spectra (CD₂Cl₂, 298 K) of the reaction mixture at $t = 150$ min of (a) **1a** + NaBArF (1 equiv.) and MA (2 equiv.) and (b) **1b** + MA (2 equiv.). *n-hexane; **diethyl ether.

this anion compared to BArF , which in turn disfavors CH_3CN decoordination as the key step to promote chain walking. With **1b**, traces of $\text{Pd}(0)$ precipitate became visible in the NMR tube only after 4 days at room temperature, confirming that **MC4**^{MA}/ **OC**^{MA} species in these $\text{Pd}(\text{py-PYA})$ compounds are remarkably stable.

To further investigate the role of CH_3CN , an additional NMR experiment was carried out with the neutral complex **1a**, adding – besides 2 equiv. of MA and 1 equiv. of NaBArF – also 1 equiv. of CH_3CN . In this case, the resonances of **1a** disappeared immediately after the addition and were replaced by those of **1b**, as a mixture of both stereoisomers (*cis* : *trans* = 97 : 3) and those of **OC**^{MA} and the three palladacycles as well as the singlet of free acetonitrile in ratios essentially identical to those starting from **1b** (Scheme 4, Table 1 and Fig. S8†). Monitoring the reaction over time revealed that **1b** disappeared after 150 min, while **MC4**^{MA} and **OC**^{MA} remained the most abundant species present. In addition, the NOESY spectrum showed an exchange cross peak between the singlets of free acetonitrile and bound CH_3CN in **OC**^{MA} (Fig. S9†). Dynamic equilibrium might be a simple exchange between bound and free acetonitrile or ring closure of **OC4**^{MA} with the formation of the corresponding palladacycle **MC4**^{MA} and release of MeCN. In this second hypothesis, the expected exchange cross peaks are not visible due to the close proximity of the relevant NMR resonances. This reactivity is comparable to that of the cationic acetonitrile complex **1b** (see above).

Qualitatively similar results were obtained when 2, rather than 1 equiv. of acetonitrile, were added, but the disappearance of the *in situ* formed **1b** was slower. Moreover, no signals from **MC5**^{MA} or **MC6**^{MA} were detected, and **MC4**^{MA} and **OC**^{MA} were the only species present in the solution after 150 min (Fig. S12 and S13†).

Overall, these detailed NMR analyses indicate that the presence of acetonitrile markedly slows down the reaction with MA and also the chain walking process, thus increasing the amounts of **MC4**^{MA} and **OC**^{MA}. In fact, the percentage of these intermediates at $t = 150$ min increased from 71% (**1b**) to 76% (**1a** + 1 equiv. of CH_3CN) and finally to 100% (**1a** + 2 equiv. of CH_3CN) (Fig. 2 and Table S1†). Moreover, **MC4**^{MA} and **OC**^{MA} were not detected when the reaction was carried out with the *in situ* activated **1a** without the addition of acetonitrile, which are the reaction conditions applied in several catalytic systems reported in the literature.^{34,35}

These results are in line with the effect of acetonitrile on the polymerization-isomerization of 1-hexene catalyzed by neutral $\text{Pd}-(\alpha\text{-diimine})$ complexes.³⁶ It was discovered that depending on the concentration of acetonitrile in the reaction medium, it was possible to affect the selectivity of the reaction, going from fast isomerization and subsequent polymerization in the absence of CH_3CN to selective α -olefin polymerization with 1 equiv. of CH_3CN , and eventually to exclusive isomerization when a large excess (20 equiv.) of MeCN was added. Moreover, it was also demonstrated that the addition of *p*-toluonitrile activated otherwise inactive $\text{Pd}(\alpha\text{-diimine})$ complexes towards the copolymerization of ethylene with specific polar

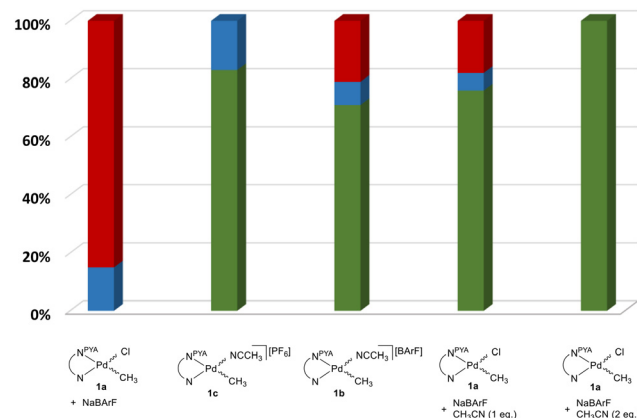


Fig. 2 Percentages of intermediates detected by NMR analysis in the reaction between **1a**, **1b** or **1c** with MA 150 min after the addition of the polar monomer; **MC4**^{MA} + **OC**^{MA} (green bars), **MC5**^{MA} (blue bars) and **MC6**^{MA} (red bars).

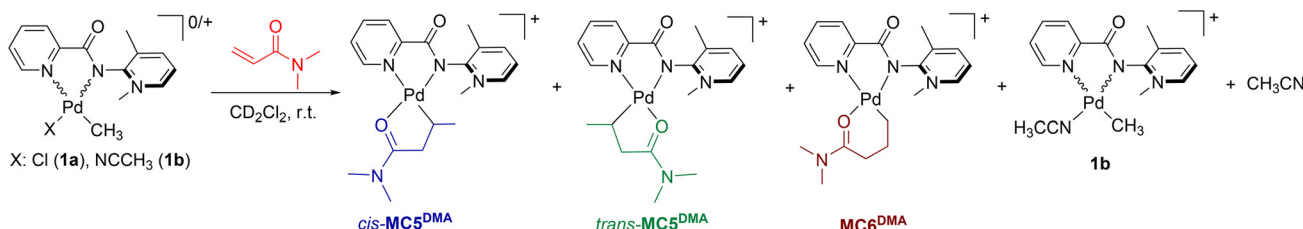
vinyl monomers, such as allyl acetate, *tert*-butyl 3-butenoate or *n*-butyl allyl ether.³¹ The results of our work strongly suggest that the nitrile coordinated to the $\text{Pd}(\text{II})$ precatalyst hampers the formation of metallacyclic intermediates, which are normally generated after the insertion of the polar monomer.

Due to the high reactivity of the neutral complex **1a** towards polar monomers, the scope of our investigation was expanded to include acrylamides. Similar to MA, the treatment of complex **1a** with DMA under the same conditions described above induced the rapid consumption of the starting complex. The ¹H NMR spectrum recorded 15 min after the addition of DMA showed the presence of two new species, assigned to the *cis* and *trans* isomers of the 5-membered metallacycle **MC5**^{DMA} in a 73 : 24 ratio.²³ The two isomers originated from DMA insertion into the $\text{Pd}-\text{CH}_3$ bond with secondary regiochemistry followed by chain walking (Scheme 5, Table 2, and Fig. S14–S18†). They were unambiguously distinguished by the chemical shift of the βCH_3 group: in *cis*-**MC5**^{DMA}, it experiences the shielding ring current from the adjacent PYA heterocycle and thus resonates at a considerably lower frequency than in *trans*-**MC5**^{DMA} (0.32 vs. 1.02 ppm). As in the corresponding MA metallacycle, for both *cis*- and *trans*-**MC5**^{DMA} the signals for a pair of diastereomers – in *ca.* equal amounts – are observed as indicated by the splitting of the βCH_3 doublets in two signals of *ca.* equal intensity. In marked contrast with the reaction of **1a** with MA, however, no signals attributable to the 4-membered palladacycle **MC4**^{DMA} were detected.

The signals of a new minor species identified as **MC6**^{DMA} slowly grew with time at the expense of **MC5**^{DMA}. Only one set of signals was clearly visible that – based on the similarity with the NMR spectrum of **MC6**^{MA} – was assigned to the *cis* isomer. Equilibrium was reached within 2 h, with a *cis*-**MC5**^{DMA} : *trans*-**MC5**^{DMA} : **MC6**^{DMA} ratio of 41 : 38 : 21 (Table S2†).

This experiment pointed out a few differences in the reaction of **1a** with the two polar vinyl monomers. Firstly, chain walking is faster with DMA than with MA once the monomer



Scheme 5 Products observed by *in situ* NMR monitoring of the reaction of complexes **1a** and **1b** with DMA.Table 2 Relative amounts, in mol%, of the compounds present in solution at $t = 15$ min after the addition of DMA to the starting mixture

Starting mixture	<i>cis</i> -MC5 ^{DMA}	<i>trans</i> -MC5 ^{DMA}	MC6 ^{DMA}	1b	Free CH ₃ CN
1a + NaBARF	73	24	3	—	—
1b	32	24	2	42	Yes

is inserted into the Pd-CH₃ bond. Secondly, once the 5-membered palladacycle **MC5** is formed, it remains the dominant species with DMA, whereas it evolves to **MC6** with MA. Finally, for all the detected palladacycles, only the *cis* isomer was observed upon MA insertion, while both *cis*- and *trans*-isomers were observed for **MC5^{DMA}**. This latter feature can be explained by the specific coordination properties of the two functional groups, amides *vs.* esters. Textbook coordination chemistry suggests that the major isomer is the most stable, *i.e.* the one where the weaker donor atom is *trans* to the group with the larger *trans*-influence. By considering that the carbonyl oxygen in amides is more basic than in esters and that the N atom of the PYA ring has a larger *trans*-influence than the pyridyl-N atom, the isomer distribution suggests that the carbanion has donor properties comparable to the amide oxygen but larger than the ester oxygen. This is also reflected in the distinct reactivity of the DMA- and MA-metallacycles (see below).

Consistent with the reactivity towards MA, complex **1b** reacts more slowly than **1a** + NaBARF also with DMA: in fact, after 15 min the major species present was unreacted **1b** (42%) together with *cis*- and *trans*-**MC5^{DMA} (32:24) and traces of **MC6^{DMA}** (2%, Table 2 and Fig. S19†). However, in contrast with the reaction with MA, with DMA full conversion of **1b** took more than 5 h (*vs.* 30 min with MA, Fig. S19†). After 5 h, the three products, *cis*- and *trans*-**MC5^{DMA} and **MC6^{DMA}**, were present in solution at the same ratio as in the reaction of **1a** with DMA (Fig. S19 and Table S2†), further confirming the high stability of the DMA-derived metallacycles. In no case were the resonances of the 4-membered palladacycle, **MC4^{DMA}**, and/or those of the corresponding open-chain intermediate observed.****

The high stability of **MC5^{DMA}** was exploited to grow single crystals. The diffusion of *n*-hexane at 4 °C into a CD₂Cl₂ mixture of **MC5^{DMA}** and **MC6^{DMA}** afforded crystals suitable for X-ray analysis. Successful acquisition and processing of the crystallographic data showed that the asymmetric unit

contains a molecule of [*trans*-**MC5^{DMA}][BARF], which is the minor isomer present in solution (Fig. 3). This is the first structurally characterized palladacycle obtained from insertion of DMA into a Pd(II)-CH₃ bond, followed by chain walking.**

The Pd(II) ion in *trans*-**MC5^{DMA}** displays the classical square planar coordination geometry with the chelating PYA ligand opposite to the 5-membered C⁴O metallacycle. The bond lengths and angles around the metal center are in line with the values observed in other Pd(II) complexes containing a pyridyl-PYA ligand.^{26,30} The Pd-N_{PYA} bond is considerably longer than the Pd-N_{pyr} bond (Pd-N2 2.121(8) *vs.* 2.027(7) Å for Pd-N1), in agreement with the higher *trans* influence of the alkyl ligand compared to the amide donor. The PYA ring is essentially orthogonal to the Pd coordination plane, with a dihedral angle of 86.1(3)°, thus minimizing steric clashes between the pyridinium *ortho*-CH₃ groups and the adjacent carbonyl group. The exocyclic C13-N2 bond length is 1.353(1) Å, much shorter than typical C-N single bonds (1.48 Å) and also shorter than in the protonated ligand (1.401(4) Å), yet longer than in the free deprotonated pyridyl-PYA ligand (1.333

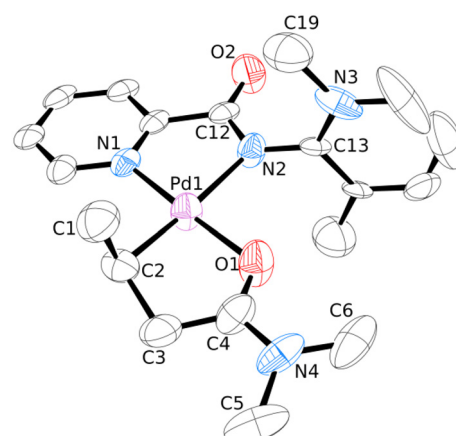


Fig. 3 ORTEP drawing (50% probability ellipsoids) of the cationic species *trans*-**MC5^{DMA}. Hydrogen atoms and the BARF anion have been omitted for the sake of clarity. Selected bond distances (Å) and angles (°): Pd1-C2 1.998(9), Pd1-N1 2.027(7), Pd1-N2 2.121(8), Pd1-O1 2.032(7), C1-C2 1.511(1), C2-C3 1.608(1), C3-C4 1.490(2), C4-O1 1.259(1), C4-N4 1.305(1), C5-N4 1.505(2), C6-N4 1.416(2), C12-O2 1.200(1), C12-N2 1.335(1), C13-N2 1.353(1), C13-N3 1.362(1), C19-N3 1.541(2), C2-Pd1-O1 83.5(4), N1-Pd1-N2 79.7(3), C1-C2-C3 106.5(9), C1-C2-Pd1 105.4(7), C4-N4-C5 119.8(1), C4-N4-C6 121.0(1), C5-N4-C6 119.0(1), [N^{PYA}]⁺-[Pd1] 86.1(3), [N^{DMA}]⁺-[Pd1] 8.9(5).**



(1) Å).^{26,30} While the orthogonal arrangement of the Pd-amide and the pyridinium ring planes should, in principle, exclude the presence of an exocyclic N≡C double bond, the short distance suggests considerable attractive forces.^{26,30} The nitrogen atom of the inserted DMA, N4, shows pronounced sp^2 hybridization with C–N–C angles of about 120°, while the C1–C2–Pd1 angle of 105.4(7)° is in agreement with the sp^3 hybridization of C2.

Saturation of a CD_2Cl_2 solution containing a mixture of **MC5^{DMA}** and **MC6^{DMA}** with ethylene at room temperature did not induce any insertion or other reaction, indicating that under these conditions, ethylene is unable to cleave the metallacycle (Fig. S20†). In contrast, the saturation of this solution with CO for 5 min led to an immediate color change of the solution from yellow to pink, without any observable formation of solid Pd(0). In the 1H NMR spectrum recorded 5 min after the exposure to CO, signals of very low intensity for **MC6^{DMA}** and **MC5^{DMA}** were still observed together with two sets of new resonances (Fig. S21†). The new species showed cross peaks in the 1H , ^{13}C HMBC spectrum between two signals in the carbonyl region at 219.9 ppm (major species) and 218.4 ppm (minor), and two pairs of βCH_3 doublets, pairwise almost equally intense: those of the major species are well-resolved at 0.79 and 0.92 ppm, whereas those of the minor one are partially overlapped at *ca.* 1.11 ppm (Fig. S25†). These findings clearly identify the new species as the *cis*- and *trans*-isomers of the Pd-acyl complex, **OC^{CODMA}** (Scheme 6),³⁷ resulting from the opening of the isomeric **MC5^{DMA}** metallacycles by CO coordination, followed by its insertion into the Pd–alkyl bond. It is reasonable to expect that another molecule of carbon monoxide is coordinated at the fourth coordination site of palladium, leading to the Pd-acyl-carbonyl derivative.

Both *cis*- and *trans*-**OC^{CODMA}** isomers exist as a pair of almost equally abundant diastereomers. The most intense βCH_3 doublets at 0.79 and 0.92 ppm were assigned to the two diastereomers of the most abundant *cis* isomer (*cis* : *trans* = 72 : 28). The presence of the diastereomers is also confirmed by the four singlets for the inserted DMA $N(CH_3)_2$ groups (between 2.97 and 3.22 ppm). In 1H , 1H -NOESY spectrum, the four βCH_3 doublets are pairwise connected by exchange cross peaks (Fig. S26†), indicating that the *cis* and *trans* isomers are in equilibrium at a slow rate on the NMR time scale at room

temperature. An analogous behavior was observed by us for Pd-methyl complexes with pyridine-imidazoline ligands, with the exchange process taking place through the cleavage of one N-arm of the chelating nitrogen donor ligand.³⁷

Finally, **OC^{CODMA}** is inert towards free ethylene and no signals derived from the insertion reaction were observed even after several hours.

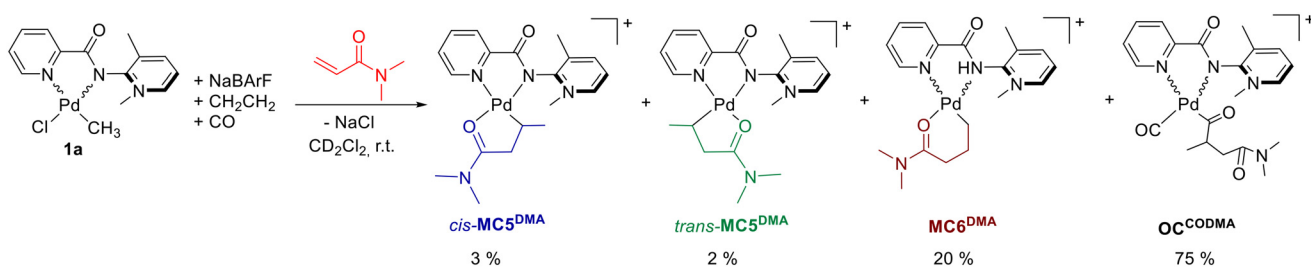
3. Conclusion

The neutral Pd(II) complex containing the PYA ligand **L10**, $[Pd(CH_3)Cl(L10)]$ (**1a**), and its monocationic derivative, $[Pd(CH_3)(NCCH_3)L10][BArF]$ (**1b**) – as a mixture of *cis* and *trans* isomers – were used to investigate by NMR spectroscopy their reactivity with methyl acrylate (MA) and *N,N*-dimethylacrylamide (DMA) as polar vinyl monomers of industrial interest.

The simultaneous addition of one equiv. of MA and NaBArF to a CD_2Cl_2 solution of **1a** led to its immediate conversion into a mixture of 4-, 5- and 6-membered metallacycles (**MC4^{MA}**, **MC5^{MA}** and **MC6^{MA}**, respectively) originating from the migratory insertion reaction of the polar monomer into the Pd–CH₃ bond, followed by chain walking. When DMA was used instead of MA, the 5-membered palladacycle **MC5^{DMA}** was preferentially formed, with only traces of **MC6^{DMA}**, whereas **MC4^{DMA}** was not detected.

The reaction of the cationic complex **1b** with MA required a 10-fold longer time for its complete conversion and afforded predominately a 4-membered palladacycle, **MC4^{MA}**, and its corresponding open-chain species, **OC^{MA}**, whereas **MC5^{MA}** and **MC6^{MA}** were present as minor species only. Similar results were obtained when progressive equivalents of acetonitrile were added to the solution of the neutral complex **1a** containing also 1 equiv. each of NaBArF and MA. Consistent with these results, the reaction of **1b** with DMA was even slower, its signals being still observed up to 5 h together with the resonances of the 5-membered metallacycle, **MC5^{DMA}**, whereas **MC6^{DMA}** was present in traces. The final product distribution at equilibrium was independent of the nature of the starting compound, **1a** or **1b**.

For each MA metallacycle, only the *cis* isomer was detected, whereas **MC5^{DMA}** formed as a mixture of *cis* and *trans* isomers.



Scheme 6 *In situ* NMR-monitored reaction of **1a** with NaBArF, DMA, ethylene and carbon monoxide. The relative amounts, in mol %, of the compounds present in solution 5 min after bubbling of CO are indicated.

In addition, it was possible to detect that both **MC5^{MA}** and the two geometrical isomers of **MC5^{DMA}** form as a pair of diastereomers.

For both polar vinyl monomers, the migratory insertion reaction into the Pd-CH₃ bond and the chain walking process are faster on the neutral compound than on the cationic complex, indicating that acetonitrile competes with the polar monomer for the coordination to palladium, playing a role in determining the microstructure of the produced macromolecules. Since most of the precatalysts investigated so far in the copolymerization of ethylene with MA are neutral Pd(II) complexes of the general formula [Pd(N-N)(CH₃)Cl] activated *in situ* upon the addition of NaBArF, it cannot be ruled out that copolymers with a different microstructure might be obtained by simply moving from the neutral to the cationic Pd-acetonitrile precatalysts. Our work indicates that acetonitrile coordination prevents β -hydrogen elimination from the growing polymer chain, which is required for the chain walking, thus hampering branching and favoring the formation of linear macromolecules.

Finally, in contrast with ester-derived metallacycles, the DMA-derived 5-membered metallacycle **MC5^{DMA}** did not react with ethylene under mild reaction conditions. This behavior is consistent with the findings about the different donor properties of the amide and the ester oxygen atoms and allows us to rationalize the different catalytic behavior of [Pd-(N-N)] complexes in the copolymerization of ethylene with either acrylic esters or amides.

Nevertheless, **MC5^{DMA}** was cleaved by carbon monoxide, thus giving rise to the possibility of using these complexes as catalysts for DMA/CO copolymerization.

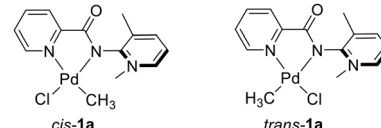
4. Experimental

General information

All complex manipulations were performed using standard Schlenk techniques under argon. Anhydrous dichloromethane was freshly obtained by distillation over CaH₂ under an argon atmosphere. The neutral pyridyl-PYA **L10** and the cationic palladium complex [Pd(CH₃)(NCCH₃)(**L10**)]⁺[PF₆⁻] (**1c**) were prepared according to a literature procedure.^{30,32} Deuterated solvents (Cambridge Isotope Laboratories, Inc. (CIL)) were stored as recommended by sellers. Ethylene (purity \geq 99.9%) supplied by SIAD and methyl acrylate (99.9%, with 0.02% of hydroquinone monomethyl ether) and *N,N*-dimethylacrylamide (99%, with 500 ppm of hydroquinone monomethyl ether) supplied by Merck were used as received. One- and two-dimensional NMR spectra were recorded on a Varian 500 spectrometer (500 MHz for ¹H, 125.68 MHz for ¹³C). The resonances are reported in ppm (δ) and referenced to the residual solvent peak *versus* Si(CH₃)₄: CD₂Cl₂ at δ 5.32 (¹H) and δ 54.00 (¹³C). ¹⁹F NMR spectra were recorded on a Varian 400 spectrometer at 376.3 MHz and referenced with respect to CCl₃F. ¹¹B NMR spectra were recorded on a Bruker 400 MHz spectrometer at 128 MHz and referenced with respect to BF₃·OEt₂.

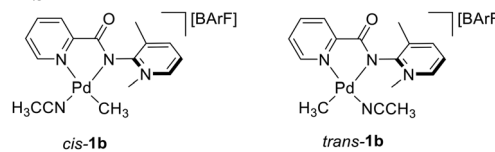
NMR experiments were performed employing the automatic software parameters. In the case of NOESY experiments, a mixing time of 500 ms was used.

Synthesis and NMR characterization of the neutral complex **1a**



The neutral PYA ligand **L10** (182 mg, 0.80 mmol) and [Pd(cod)(CH₃)Cl] (212 mg, 0.8 mmol) were dissolved in dry CH₂Cl₂ (5 mL). The resulting yellow mixture was stirred for 2 h at 23 °C and then concentrated to 2 mL. Upon addition of Et₂O (6 mL), a precipitate formed, which was filtered and washed with additional Et₂O. The precipitation from CH₂Cl₂ and Et₂O was repeated until no palladium precursor was detected anymore. Then the precipitate was dried under vacuum to afford **1a** as a bright yellow solid consisting of a mixture of *cis* and *trans* isomers in a 4:1 ratio (285 mg, 92%). The isomers were unambiguously identified by ¹H NOE NMR spectroscopy. Spectroscopic data for *cis*-**1a**: ¹H NMR (500 MHz, CD₂Cl₂, 298 K) δ = 8.98 (d, $^3J_{HH}$ = 4.8 Hz, 1H, H⁶), 8.22–8.11 (m, 2H, H_{PYA}), 8.06–7.93 (m, 2H, H_{pyr}), 7.63–7.51 (m, 1H, H_{pyr}), 7.43 (dd, $^3J_{HH}$ = 7.2, 6.7 Hz, 1H, H_{PYA}), 4.25 (s, 3H, NCH₃), 2.50 (s, 3H, PYA-CH₃), -0.24 (s, 3H, Pd-CH₃) ppm. ¹³C{¹H} NMR (75 MHz, CD₂Cl₂, 298 K) δ = 169.93 (CO), 160.45 (C_{PYA}), 150.96 (C_{pyr}), 147.76 (CH_{PYA}), 145.62 (CH_{PYA}), 140.49 (CH_{PYA}), 138.64 (CH_{pyr}), 138.04 (C_{PYA}-Me), 127.80 (CH_{pyr}), 124.68 (CH_{pyr}), 121.67 (CH_{PYA}), 44.63 (NCH₃), 18.35 (PYA-CH₃), -11.40 (Pd-CH₃) ppm. Spectroscopic data for *trans*-**1a**: ¹H NMR (500 MHz, CD₂Cl₂, 298 K) δ = 8.49 (d, $^3J_{HH}$ = 4.8 Hz, 1H, H⁶), 8.22–8.11 (m, 1H, H_{pyr}), 8.06–7.93 (m, 3H, H_{pyr} + 2 H_{PYA}) 7.63–7.51 (m, 1H, H_{pyr}), 7.26 (dd, $^3J_{HH}$ = 7.2, 6.7 Hz, 1H, H_{PYA}), 4.27 (s, 3H, NCH₃), 2.46 (s, 3H, PYA-CH₃), 0.81 (s, 3H, Pd-CH₃) ppm. ¹³C{¹H} NMR (75 MHz, CD₂Cl₂, 298 K) δ = 160.52 (C_{PYA}), 147.17 (CH_{pyr}), 144.17 (CH_{PYA}), 139.72 (CH_{PYA}), 138.62 (CH_{pyr}), 136.52 (C_{PYA}-Me) 127.55 (CH_{pyr}), 126.40 (CH_{pyr}), 119.93 (CH_{PYA}), 45.00 (NCH₃), 18.65 (PYA-CH₃), -1.32 (Pd-CH₃) ppm. The remaining quaternary carbons were not resolved. HR-MS (*m/z*): found: 389.0614; calculated for C₁₆H₁₉N₄OPd [M - Cl + MeCN]⁺ = 389.0594. Elemental analysis calculated for C₁₄H₁₆ClN₃OPd \times 0.2CH₂Cl₂ (%): C 42.52; H 4.12; N 10.47 found: C 42.58; H 4.10; N 10.53.

Synthesis and NMR characterization of the cationic complex **1b**



To a stirred solution of **1a** in dry CH₂Cl₂ (0.1 mmol in 5 mL), at room temperature, a solution of CH₃CN (1 mL) and NaBArF (1.15 eq.) was added. The reaction mixture was stirred in the dark for 1 h. Afterward, it was filtered on Celite and concen-



trated to a few milliliters of volume and upon addition of cold Et_2O and *n*-hexane, a white solid precipitate formed, which was filtered and dried under vacuum for 12 h at 277 K to afford complex **1b** as an off-white solid (99 mg, yield = 78%). NMR analysis revealed the presence of two isomers in a 19:1 *cis* to *trans* ratio. The isomers were unambiguously identified by ^1H NOE NMR spectroscopy.

Spectroscopic data for *cis*-**1b**: ^1H NMR (500 MHz, CD_2Cl_2 , 298 K) δ = 8.36 (m, 1H, H^6), 8.23–8.18 (m, 2H, 2 H_{PYA}), 8.15–8.11 (m, 1H, H_{PYA}), 8.09 (td, 1H, H^3), 7.73–7.70 (m, 8H, $\text{H}_{\text{ortho BArF}}$), 7.66 (dt, 1H, H^5), 7.56 (s, 4H, $\text{H}_{\text{para BArF}}$), 7.55–7.51 (m, 1H, H^4), 4.16 (s, 3H, NCH_3), 2.46 (s, 3H, PYA-CH_3), 2.40 (s, 3H, NCCH_3), −0.06 (s, 3H, Pd-CH_3) ppm. $^{13}\text{C}\{^1\text{H}\}$ NMR (101 MHz, CD_2Cl_2 , 298 K) δ = 170.29 (CO), 162.17 (q, $^1\text{J}_{\text{C-B}} = 49.7$ Hz, $\text{C}_{\text{ipso BArF}}$), 158.96 (C_{PYA}), 150.28 (C_{pyr}), 147.56 (C_{α}), 146.78 (CH_{pyr}), 141.18 (CH_{pyr}), 140.27 (C_γ), 138.46 ($\text{C}_{\text{PYA-Me}}$), 135.22 ($\text{C}_{\text{ortho BArF}}$), 129.27 (q, $^2\text{J}_{\text{C-F}} = 31.4$ Hz, C-CH_3), 128.73 (C_β), 126.37 (CH_{pyr}), 124.83 (q, $^1\text{J}_{\text{C-F}} = 272.4$ Hz, CF_3), 123.01 (CH_{pyr}), 120.95 (Pd-NCCH_3), 117.89 ($\text{C}_{\text{para BArF}}$), 44.70 (NCH_3), 18.32 (PYA-CH_3), 3.84 (CH_3CN), −6.46 (Pd-CH_3) ppm. $^{19}\text{F}\{^1\text{H}\}$ NMR (376 MHz, CD_2Cl_2 , 298 K) δ = −62.89 ppm. $^{11}\text{B}\{^1\text{H}\}$ NMR (128 MHz, CD_2Cl_2) δ = −6.60 ppm. Spectroscopic data for *trans*-**1b**: ^1H NMR (500 MHz, CD_2Cl_2 , 298 K) δ = 8.42–7.44 (m, 7H, H_{pyr} , H_{PYA}), 7.73–7.70 (m, 8H, $\text{H}_{\text{ortho BArF}}$), 7.56 (s, 4H, $\text{H}_{\text{para BArF}}$), 4.21 (s, 3H, NCH_3), 2.56 (s, 3H, PYA-CH_3), 2.36 (s, 3H, Pd-NCCH_3), 1.02 (s, 3H, Pd-CH_3). Aromatic ^1H signals were not resolved. ^{13}C data were not resolved due to low intensity. HR-MS (*m/z*): found: 389.0596; calculated for $\text{C}_{16}\text{H}_{19}\text{N}_4\text{OPd}$ $[\text{M} - \text{BArF}_2]^{+}$ = 389.0594. Elemental analysis calculated for $\text{C}_{48}\text{H}_{31}\text{BF}_{24}\text{N}_4\text{OPd}$ (%): C 46.01; H 2.49; N 4.47 found: C 45.46; H 2.31; N 4.01.

General procedure for the *in situ* NMR reactivity of **1a** with polar vinyl monomers

A 10 mM or 20 mM CD_2Cl_2 solution of **1a** was prepared and its NMR spectrum was recorded. Then to this pale-yellow solution, a solution of 1 equiv. of NaBArF and 2 equiv. of the polar monomer (MA or DMA) was added. The precipitation of NaCl was immediately observed. The reaction was followed over time, at room temperature, by NMR spectroscopy.

General procedure for the *in situ* NMR reactivity of **1b** with polar vinyl monomers

To 10 mM or 20 mM CD_2Cl_2 solution of **1b**, 2 equiv. of the polar vinyl monomer (MA or DMA) was added. The reaction was followed over time, at room temperature, by NMR spectroscopy.

General procedure for the *in situ* NMR reactivity of **1a** with NaBArF , DMA and gaseous monomers

2 h after the addition of NaBArF (1 equiv.) and DMA (2 equiv.) to a 20 mM CD_2Cl_2 solution of **1a**, the solution was saturated with ethylene and NMR spectra were recorded, at room temperature, for 1 h. Afterward, the solution was saturated with carbon monoxide. Its color changed from pale yellow to pale

pink. The reaction was followed over time, at room temperature, by NMR spectroscopy.

Author contributions

The manuscript was written through contributions of all authors.

Data availability

The data supporting this article have been included as part of the ESI.†

Crystallographic data for *trans*-**MC5^{DMA}** have been deposited at the Cambridge Crystallographic Data Centre (CCDC) under 2386206.†

Conflicts of interest

There are no conflicts to declare.

Acknowledgements

This work was supported by the Università degli Studi di Trieste (B. M., G. B., and C. A.: FRA 2022). The PhD fellowship of C. A. was supported by FSE-PO 2014/2020 and Regione FVG, Program 89/19. E. R. and M. A. thank the Swiss National Science Foundation for generous financial support (grants 200020-182663 and 200020-212863). We thank Dr Maurizio Polentarutti for the technical assistance provided by Elettra – Sincrotrone Trieste in Area Science Park.

References

- 1 B. P. Carrow and K. Nozaki, *Macromolecules*, 2014, **47**, 2541–2555.
- 2 C. Tan, C. Zou and C. Chen, *Macromolecules*, 2022, **55**, 1910–1922.
- 3 H. Zheng, Z. Qiu, D. Li, L. Pei and H. Gao, *J. Polym. Sci.*, 2023, **61**, 2987–3021.
- 4 Z. Song, S. Wang, R. Gao, Y. Wang, Q. Gou, G. Zheng, H. Feng, G. Fan and J. Lai, *Polymers*, 2023, **15**, 4343.
- 5 Y. Zhao, Z. Zhang and Y. Luo, *Inorganics*, 2024, **12**, 233.
- 6 L. Guo, S. Dai, X. Sui and C. Chen, *ACS Catal.*, 2016, **6**, 428–441.
- 7 Y. Zhang, Y. Zhang, X. Hu, C. Wang and Z. Jian, *ACS Catal.*, 2022, **12**, 14304–14320.
- 8 L. K. Johnson, S. Mecking and M. Brookhart, *J. Am. Chem. Soc.*, 1996, **118**, 267–268.
- 9 Z. Chen and M. Brookhart, *Acc. Chem. Res.*, 2018, **51**, 1831–1839.
- 10 F. Wang and C. Chen, *Polym. Chem.*, 2019, **10**, 2354–2369.



11 E. Drent, R. van Dijk, R. van Ginkel, B. van Oort and R. I. Pugh, *Chem. Commun.*, 2002, 744–745.

12 A. Nakamura, T. M. J. Anselment, J. Claverie, B. Goodall, R. F. Jordan, S. Mecking, B. Rieger, A. Sen, P. Van Leeuwen and K. Nozaki, *Acc. Chem. Res.*, 2013, **46**, 1438–1449.

13 L. Guo, J. Li, W. Zhao, P. Wei, Y. Ju, X. Cui, L. Yuan, M. Ji and Z. Liu, *Inorg. Chem.*, 2024, **63**, 17809–17827.

14 X. Wu, J. Jiang, M. Zou, H. Wang and S. Dai, *Polymer*, 2024, **312**, 127617.

15 Y. Zhang, C. Wang, S. Mecking and Z. Jian, *Angew. Chem., Int. Ed.*, 2020, **59**, 14296–14302.

16 Y. Zhang and Z. Jian, *Macromolecules*, 2020, **53**, 8858–8866.

17 S. Dai, X. Sui and C. Chen, *Angew. Chem., Int. Ed.*, 2015, **54**, 9948–9953.

18 S. Dai, S. Zhou, W. Zhang and C. Chen, *Macromolecules*, 2016, **49**, 8855–8862.

19 M. Li, X. Wang, Y. Luo and C. Chen, *Angew. Chem., Int. Ed.*, 2017, **56**, 11604–11609.

20 S. Dai and C. Chen, *Angew. Chem., Int. Ed.*, 2016, **55**, 13281–13285.

21 F. Zhai, J. B. Solomon and R. F. Jordan, *Organometallics*, 2017, **36**, 1873–1879.

22 C. Alberoni, M. C. D'Alterio, G. Balducci, B. Immirzi, M. Polentarutti, C. Pellecchia and B. Milani, *ACS Catal.*, 2022, **12**, 3430–3443.

23 T. Friedberger, P. Wucher and S. Mecking, *J. Am. Chem. Soc.*, 2012, **134**, 1010–1018.

24 S. R. Gaikwad, S. S. Deshmukh, V. S. Koshti, S. Poddar, R. G. Gonnade, P. R. Rajamohanan and S. H. Chikkali, *Macromolecules*, 2017, **50**, 5748–5758.

25 Y. Zhang, H. Mu, L. Pan, X. Wang and Y. Li, *ACS Catal.*, 2018, **8**, 5963–5976.

26 M. Navarro, V. Rosar, T. Montini, B. Milani and M. Albrecht, *Organometallics*, 2018, **37**, 3619–3630.

27 J. J. Race and M. Albrecht, *ACS Catal.*, 2023, **13**, 9891–9904.

28 W. Zhang, P. M. Waddell, M. A. Tiedemann, C. E. Padilla, J. Mei, L. Chen and B. P. Carrow, *J. Am. Chem. Soc.*, 2018, **140**, 8841–8850.

29 A. Dall'Anese, V. Rosar, L. Cusin, T. Montini, G. Balducci, I. D'Auria, C. Pellecchia, P. Fornasiero, F. Felluga and B. Milani, *Organometallics*, 2019, **38**, 3498–3511.

30 G. M. Ó. Máille, A. Dall'Anese, P. Grossenbacher, T. Montini, B. Milani and M. Albrecht, *Dalton Trans.*, 2021, **50**, 6133–6145.

31 Y. Zhang and Z. Jian, *Polym. Chem.*, 2022, **13**, 4966–4972.

32 E. Reusser and M. Albrecht, *Dalton Trans.*, 2023, **52**, 16688–16697.

33 A. Macchioni, G. Bellachioma, G. Cardaci, M. Travaglia, C. Zuccaccia, B. Milani, G. Corso, E. Zangrandi, G. Mestroni, C. Carfagna and M. Formica, *Organometallics*, 1999, **18**, 3061–3069.

34 C. Tan and C. Chen, *Angew. Chem., Int. Ed.*, 2019, **58**, 7192–7200.

35 D. Nguyen, S. Wang, L. C. Grabow and E. Harth, *J. Am. Chem. Soc.*, 2023, **145**, 9755–9770.

36 G. R. Jones, H. E. Basbug Alhan, L. J. Karas, J. I. Wu and E. Harth, *Angew. Chem., Int. Ed.*, 2021, **60**, 1635–1640.

37 A. Bastero, A. Ruiz, C. Claver, B. Milani and E. Zangrandi, *Organometallics*, 2002, **21**, 5820–5829.

